Stochastic fluid structure interaction of three dimensional plates facing a uniform flow

Olivier Cadot

Stochastic fluid structure interaction of three dimensional plates facing a uniform flow

O. CADOT†

IMSIA, ENSTA-ParisTech/CNRS/CEA/EDF, Université Paris Saclay, 828 Boulevard des Maréchaux, 91762 Palaiseau Cedex, France

(Received ?; revised ?; accepted ?. - To be entered by editorial office)

An experiment of a flat rectangular plate facing a uniform flow at Re= 264000 shows the importance on the base pressure loading of the asymmetric static modes of the turbulent wake. The plate is free to rotate around its small symmetry axis. For plates with aspect ratio $\kappa < 6$, the angular position exhibits strong random discontinuities between steady states of non zero angles. The steady states have long time durations, more than one order of magnitude larger than the convective timescale. The discontinuities, comparable to rare and violent events are due to strong fluid forces associated with the drastic global change of the three dimensional wake, mainly the switching between the static asymmetric modes. A clear transition occurs at $\kappa = 6$ for which the angular fluctuations are minimum leading for $\kappa > 6$ to a classical fluid structure interaction with periodic fluctuations. The transition is supported by a recent global stability analysis of rectangular fixed plates in the laminar regime.

1. Introduction

It is known that for three dimensional bodies, the first bifurcation in the flow solution as the Reynolds number is increased leads to steady symmetry breaking modes. This has been demonstrated for axisymmetric bodies (Fabre *et al.* 2008; Pier 2008; Bohorquez *et al.* 2011) and for bodies having rectangular blunt base (Grandemange *et al.* 2012; Marquet & Larsson 2014). At low Reynolds number, these steady modes play an important role in problems of fluid structure interaction, such as for instance the dynamics of falling bodies (Ern *et al.* 2012). Recently, steady symmetry breaking modes have been evidenced at large Reynolds numbers, leading to random multistable dynamics. For bodies having a reflectional symmetry such as the Ahmed body, Grandemange *et al.* (2013) have shown that the wake is bistable with a long time dynamics of random switching between two mirror symmetry breaking modes. These observations have been generalized to axisymmetric geometries by Rigas *et al.* (2014) and Grandemange *et al.* (2014), where the only two asymmetric states are replaced by an infinite number of asymmetric states due to the multiplicity of reflectional symmetries of the axisymmetric geometry.

As shown by Marquet & Larsson (2014), simple rectangular plates are subjected to these steady symmetry breaking modes in the laminar regime and one may wonder how they can interfere in the case of fluid structure interaction at large Reynolds numbers. The purpose of this work is to study the consequence of such static symmetry breaking modes dynamics on a very simple fluid structure interaction experiment involving a three dimensional turbulent wake.

The paper is organized as follows. Section 2 describes the flat plate geometry and the measurements. Results in Sec. 3 are presented in three parts. Section 3.1 investigates the

† Email address for correspondence: cadot@ensta.fr

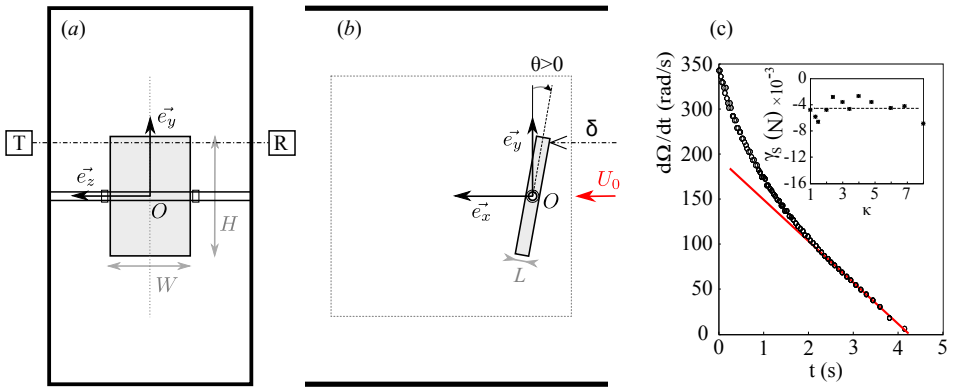

FIGURE 1. Experimental set-up. Cross section (a) and side view (b) of the hydrodynamic tunnel with the flat plate of aspect ratio $\kappa = \frac{H}{W}$. In (a) the T and R blocks sketches the optical device that measures the position δ of the plate. The dashed frame in (b) represents the area for visualizations and PIV measurements. Angular velocity (c) during the free decay in air of the plate having $\kappa = 2.4$, and solid friction torque γ_S (inlet) estimated from the linear decay displayed by the straight line.

presence of the static symmetry breaking modes for a fixed plate. The fluid structure interaction mechanism is then investigated in Sec. 3.2. The effect of the plate aspect ratio on the plate dynamics is studied in Sec. 3.3. Results are discussed with concluding remarks and perspectives in Sec. 4.

2. Experimental set-up

The mechanical system is a simple plate that rotates freely around its small reflectional symmetry axis as depicted in Fig. 1. The plate is made of plexiglass, its thickness L is 6 mm, the height H is 48 mm. The plate dimension accuracy is about 0.05 mm. Aspect ratios $\kappa = \frac{H}{W}$ ranging from 1 to 8 are investigated with plates of different widths W. The plates are pierced with a hole of 4.2 mm in diameter at the position $H/2$. The position of the hole is only accurate to 0.2 mm because it required a change of the machine tool. A rod (the axis of rotation), with a diameter of 4 mm made of brass and lubricated with silicon oil is passed through the hole. The plate is then free to rotate around a fixed axis. Two teflon annuli avoid the plate to slide along the rod. We denote θ, the angle between the plate and the vertical unit vector $\vec{e_y}$, taken as positive in the clockwise direction.

The friction torque per unit of lenght γ_S (such that the total friction torque is $\Gamma_S = \gamma_S W$) is estimated for all the plates in air. The angular velocity decay $\Omega(t)$ of the free rotating plate is measured as shown in Fig. 1(c). In that case, $I\frac{d\Omega}{dt} = \gamma_S W$, where the plate inertia is $I = \rho_p \frac{H^3}{12} WL$, and the plate density $\rho_p = 1080$ kg/m^3. For all the plates, the velocity decrease becomes linear for $\Omega < 100$ rad/s (the typical angular velocity never exceeds 20 rad/s in the following experiments). We find (see Fig. 1c, inlet), that $\gamma_S \simeq -4 \times 10^{-3}$ N for all plates.

The dynamical system is placed in a hydrodynamic tunnel of cross section 150×80 mm. The test section is 800 mm long and completely transparent. The fluid is water ($\rho = 1000$ kg/m^3). The main flow velocity is set to $U_0 = 5.5$ m s^{-1}, such that the Reynolds number defined as Re$= \frac{U_0 H}{\nu} = 264000$. There is no cavitation in the flow except during visualizations for which the pressure in the tunnel is reduced to produce enough bubbles to seed the wake.

To determine the importance of the friction on the plate dynamics in the uniform

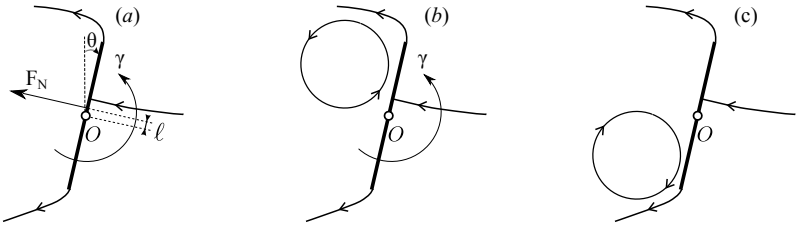

FIGURE 2. Illustration (a) of the restoring torque due to the potential flow with cavity. Sketch of the low pressure recirculation for the fixed plate (b) and steady state of the free plate with no net torque (c).

water flow, it is convenient to estimate the hydrodynamic torque γ from that of an oblique 2-dimensional flat plate using the inviscid wake model (Wu 1956). The theory gives $\gamma = -\ell(\theta)F_N(\theta)$, where $\ell(\theta) \simeq \frac{1.8}{7\pi}H\theta$ is the distance from the axis of rotation to the application point of the normal force $F_N(\theta) = \frac{1}{2}\rho U_0^2 H \frac{2\pi\cos\theta}{4+\pi\cos\theta}(1+\sigma)$ as sketched in Fig. 2(a). For small angular deviations

$$\gamma(\theta) \simeq -\frac{\pi}{4+\pi}\rho U_0^2 H(1+\sigma)\ell(\theta) = -C(1+\sigma)\theta, \tag{2.1}$$

thus defining a hydrodynamic stiffness $C = 88\times10^{-3}$ N/° taking the cavity number (i.e. base suction) $\sigma = 0$ which corresponds to the Helmholtz wake that minimizes the normal force. At an inclination of 1°, the hydrodynamic torque γ is one order of magnitude larger than the friction torque γ_S, friction is then negligible for angular positions $\theta > 1°$.

A Pegasus dual pulse 8 mJ Nd:YLF laser and a camera Photron APX RS with a resolution of 1024 × 1024 pixels are employed for Particle Image Velocimetry (PIV) measurements using the Lavision software. The setup acquires image pairs at a rate of $f_{\rm acq} = 60$ Hz, corresponding to the dimensionless frequency $f^*_{\rm acq} = f_{\rm acq}\frac{H}{U_0} = 0.52$. Conventional notations for the velocity components will be used, say (u, v, w) in the coordinate system $(\vec{e}_x, \vec{e}_y, \vec{e}_z)$. The measurements area of the velocity field (plane $z = 0$ that gives access to u and v) is displayed in Fig. 1(b). The thickness of the laser light sheet is about 3 mm. The interrogation window size is 32×32 pixels with an overlap of 50%. The window corresponds to physical sizes of 3.6 × 3.6 mm. For simultaneous measurements with the plate angle, θ is deduced from the acquired frames. The resolution is then limited by the pixel density of the camera to $\Delta\theta = \pm0.15°$, and the sampling frequency of the angle is also 60 Hz. For the flow visualizations, the shutter of the camera is set to $f_{\rm acq} = 60$ Hz and the repetition rate of the laser to 2 kHz. As a result, bubble trajectories reveal the flow structure over a non dimensional duration of $dt^* = 1/f^*_{\rm acq} = 1.91$.

For accurate measurements of the angle, a high speed and high precision optical Keyence micrometer (LS-7070M) constituted by a transmission unit which emits light and a receiving unit which detects the position of the shadow of the targeting object is used (see Fig. 1a). The micrometer has an accuracy of ±3 μm and a sampling frequency of 2000 Hz. In our case, it detects the horizontal position of the superior edge of the plate facing the flow as indicated by the δ position in Fig. 1(b). The estimated accuracy for the angle measurements is $\Delta\theta = \pm0.01°$.

3. Results

For the remainder of the paper, a^* denotes the non-dimensional value of any quantity $a(x, y, z, t)$ made dimensionless by a combination of the height H of the plate and the inlet velocity U_0. Time in non dimensional units is thus defined as $t^* = tU_0/H$.

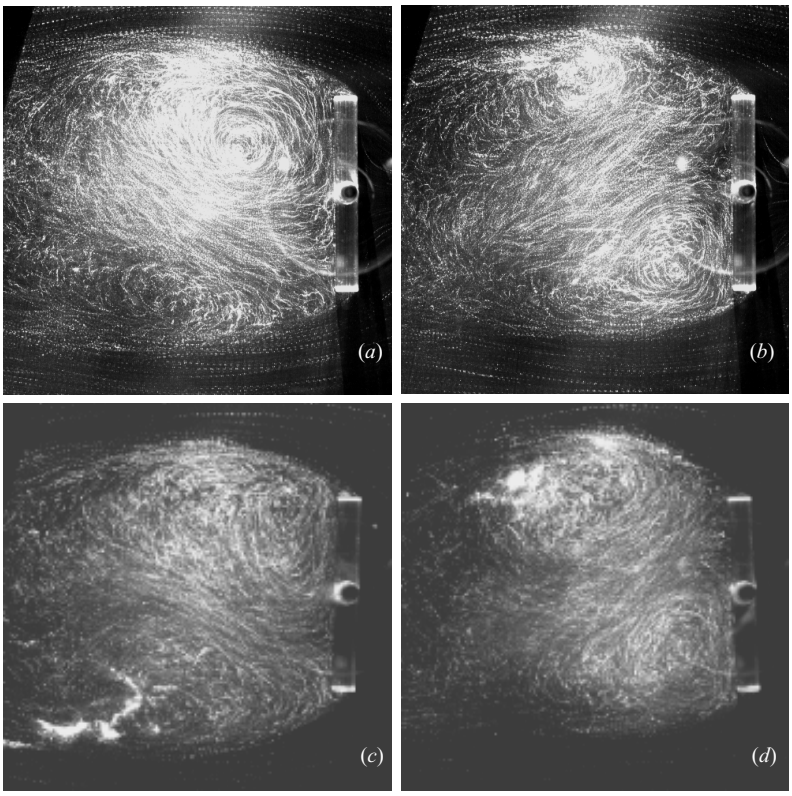

FIGURE 3. Visualizations of N (left) and P (right) states of the wake with a fixed plate. (a) and (b): $\theta = 0$ (c): $\theta > 0$, (d): $\theta < 0$.

3.1. *Fixed plate of aspect ratio* $\kappa = \frac{3}{2}$

We first study the flow dynamics of the fixed plate using the flow visualization. The striking result is the observation for a plate angle $\theta = 0$ of an intermittency between two quasi-permanent asymmetric recirculations as displayed in Fig. 3(a,b). Their lifetime is random and can be as long as a few seconds, say few hundreds in terms of $\frac{H}{U_0}$ units. In Fig. 3(a) a circular anticlockwise recirculation is clearly visible on the upper part of the plate base, we will call this flow structure the N state of the wake. Fig. 3(b) is a mirror symmetry of Fig. 3(a), with a circular clockwise recirculation on the lower part of the base plate, it will be called the P state. The letter P for positive or N for negative refers to the sign of the vertical pressure gradient at the plate base following the same terminology as in Grandemange *et al.* (2013). The sign can be guessed from the visualization because the circular recirculation is a source of low pressure, it will be confirmed later in the paper when the free plate will be investigated.

These two coherent wake states can be quasi-permanently forced by breaking the top-bottom symmetry with a small inclination angle $\theta \neq 0$. In Fig. 3(c) the state N is forced by a small positive angle while in Fig. 3(d) the state P is forced with a small negative angle. It is worth mentioning that for both cases the base pressure gradient introduces a torque having the same sign as that of the torque in (2.1) resulting from the front pressure distribution. Hence both front and base pressure distributions contribute constructively to a positive stiffness as illustrated by the scheme in Fig. 2(b).

The long time dynamics is better quantified using the velocity field measurements,

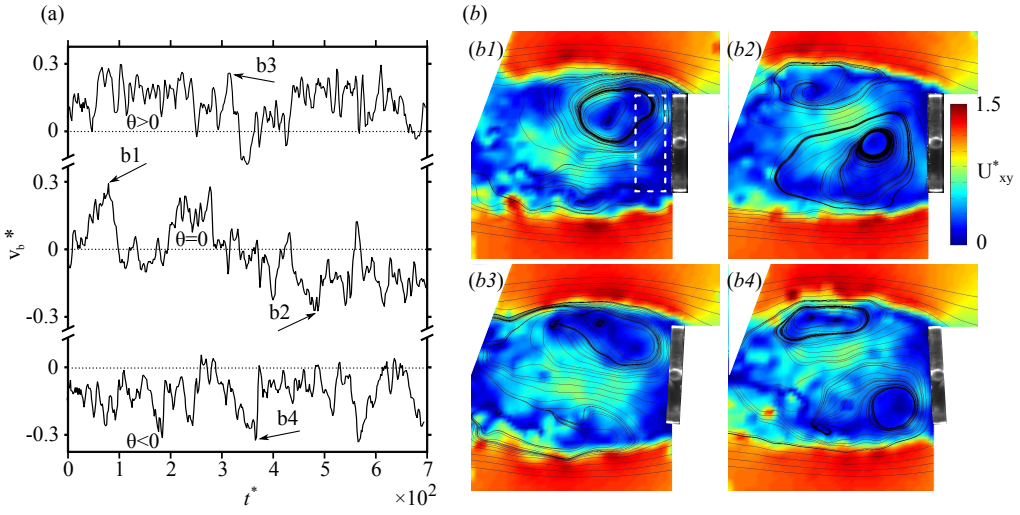

FIGURE 4. Time series (a) of the base vertical velocity v_b^* of the fixed plate for, from top to bottom $\theta > 0; = 0; < 0$. The letters b1 to b4 correspond respectively to the instantaneous PIV fields in (b) labeled $(b1)$ to $(b4)$. Velocity fields are displayed with streamlines (black lines) and velocity modulus U_{xy} (color map) in (x, y) plane. The dashed rectangle in (a) is the integration area for the base velocity computation v_b^* in (3.1).

especially looking at the time series of the base velocity displayed in Fig. 4(a) for 3 fixed angles defined as :

$$v_b^* = \int_{-1/2}^{+1/2} dy^* \int_{1/10}^{1/3} dx^* v^* \tag{3.1}$$

The bounding box size at the base is displayed on the instantaneous PIV field in Fig. 4$(b1)$. For the vertical plate ($\theta = 0$), the base velocity in Fig. 4(a) explores both positive and negative values, but strikingly it is able to keep the same sign during long time durations, about 100 non dimensional units, thus confirming the previous visualizations. As expected, the positive base velocity event labeled b1 in Fig. 4(a) is associated with an instantaneous N state in Fig. 4$(b1)$ and the negative base velocity event b2, with an instantaneous P state in Fig. 4$(b2)$. For both cases of a small inclination angle, the base velocity keeps the same sign most of the time corresponding instantaneously to either the N state for the positive angle and positive base velocity (Fig. 4$b3$) or to the P state for the negative angle and negative base velocity (Fig. 4$b4$).

3.2. *Free plate of aspect ratio* $\kappa = \frac{3}{2}$

When the plate is free to rotate, it orientates itself almost perpendicularly to the flow direction (the horizontal position has a negative stiffness and is consequently unstable). The base velocity and the angle are simultaneously measured using the PIV set-up. Both time series are displayed in Fig. 5 over a non dimensional time duration of 350.

The plate dynamics appears to be very singular, with discontinuities corresponding to high angular velocities. We can see that each of the large angular velocities $\frac{d\theta}{dt}$ is correlated to an extreme base velocity v_b^*. Some of the large deviation events are bringing the system toward large $|\theta|$, such as during the periods $[o1, o2]$ or $[o3, o4]$ while others are bringing the system back to small $|\theta|$ such as during the period $[b1, b2]$ or $[b3, b4]$.

The wake is first investigated during deviations departing from $\theta = 0$ in Fig. 6$(o1 - o4)$. In these figures, the plate picture is extracted from the PIV acquisition from which the velocity field is computed. It can be seen that the P state is present during the clockwise

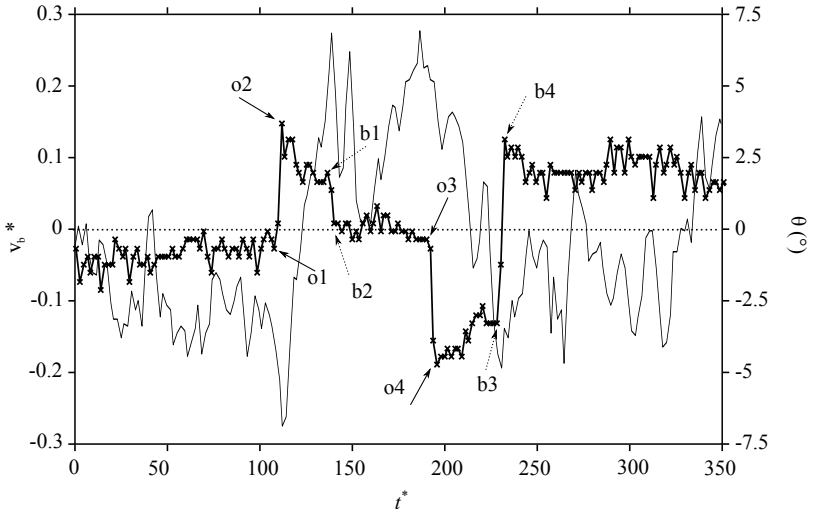

FIGURE 5. Angular position θ (crossed line) and base velocity (smooth line) vs. time extracted from the PIV acquisition. Each label refers to an instantaneous velocity field in Fig. 6.

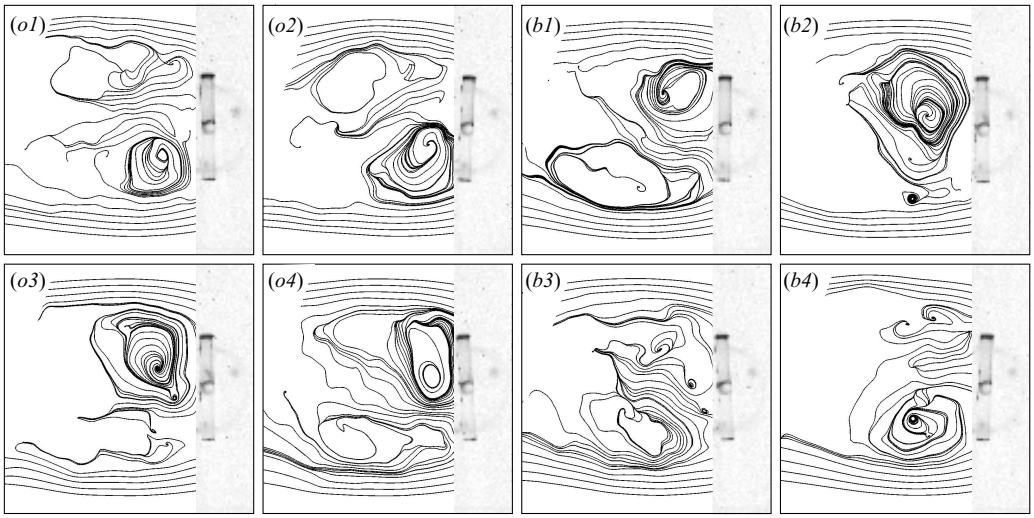

FIGURE 6. Instantaneous velocity field of the free plate. Each label refers to a time stamp denoted in Fig. 5.

motion of the plate in the phase $[o1, o2]$ with a strong negative base velocity (see Fig. 5). The clockwise motion indicates that the P state applies a positive torque on the plate. Similarly, the N state is present during the anticlockwise motion in the phase $[o3, o4]$ with a strong positive base velocity (see Fig. 5). The anticlockwise motion indicates that the N state applies a negative torque on the plate. During the phase $[o2, b1]$, the base velocity in Fig. 5 changes sign from an extreme negative value to an extreme positive value. At the instant $b1$, the wake has effectively changed to state N as can be stated from Fig6($b1$), and again a negative torque is applied due to the presence of the N state during the phase $[b1, b2]$. An identical scenario is observed during the phase $[o4, b4]$ where the base velocity changes sign again from an extreme positive value to an extreme negative value. At instant $o4$, the N state is present, while at $b3$ the state definition is not clear,

but at $b4$ the P state is clearly present indicating a positive torque producing a clockwise motion of the plate.

On the basis of these observations, the stochastic dynamics can be summarized as follows. Each state applies a torque on the plate that is able to produce an inclination angle which provokes the switching to the mirror state. For instance, the N state provokes an inclination towards large negative angles $\theta < 0$ as during the phase $[o3, o4]$, but from the fixed plate experiment, Fig. 4(d) indicates that $\theta < 0$ is the condition for the observation of the P state, not the N state. Then the probability at $o4$ to change state from N to P is very high. Indeed, the following switching revealed by the change of the base velocity sign is clearly observable during the phase $[o4, b3]$. Eventually, it is important to mention that for the cases $o2$, $o4$ and $b4$ the base pressure gradient of the wake mode introduces a torque having an opposite sign to that of the torque in (2.1) resulting from the front pressure distribution. These states, depicted in Fig. 2(c), can then correspond to stable equilibrium positions with inclined plate. The lifetime of these equilibrium positions depends on the probability of the wake to change state for a given inclination angle θ.

3.3. *Statistics and dynamics of free plates having different aspect ratio*

Plates of 12 different widths W with free rotation are successively tested to study the aspect ratio κ effect on the fluid structure mechanism evidenced above. Time series are first shown over a non dimensional duration of 1000 in Fig. 7.

At first glance, there is a huge variety of angle dynamics depending on the aspect ratio value. Discontinuities, such as those evidenced in Fig. 5 are observable for $\kappa < 6$, with maximal amplitude deviations around $\kappa = 2.4$. In this range, the dynamical system is able to keep a non zero constant angle during long non dimensional periods of 100 and sometimes even larger. The power spectra in Fig.8(a) are computed from time series acquired during a total non dimensional time of 50 000, they are averaged over 500 time units, leading to the frequency resolution $df^* = 0.002$. All the spectra obtained with aspect ratio $\kappa < 3.43$ exhibit a high energetic power law at low frequencies for $f^* < 0.2$. The exponent that varies from -2 at $\kappa = 1$ to -3 at $\kappa = 3.43$ is associated with the random appearance of discontinuities (Grandemange *et al.* 2013). Weak periodic oscillations of θ are observable in the spectra as shown by the peak at St=0.235 for $\kappa = 1$. Their frequencies are reduced to St=0.195 as the aspect ratio is increased to $\kappa = 2$ and then the periodic mode vanishes completely for aspect ratios even larger.

The probability density functions (PDFs) of the angle θ are presented in Fig.8(b). The wider distributions of angles are observed in the range $\kappa \simeq [2 - 4]$. For these cases, the distributions are rather uniform, but sometimes (as for $\kappa = 2, 3$) we can observe three weak but significant bumps. The central bump around $\theta = 0$ is larger than the two symmetric ones located on both sides.

The mean angle is generally not zero, and some unexpected asymmetry of the distributions are observable. It emphasises the sensitivity to symmetrical imperfection on the lever arm responsible for the plate dynamics, it is mainly due the accuracy in the axis position at $H/2$ (see Fig.1b and Sec.2). We made new plates to improve this accuracy. However,the little clearance of 0.2 mm between the hole diameter and the axis diameter required for low friction rotation will create by gravity a small permanent downward displacement of 0.1 mm of the plate from the origin O, thus producing a plate angle equilibrium with the uniform flow at a slightly positive value of θ.

At the aspect ratio $\kappa = 6$, the fluctuations of the angular position are minimum and a clear transition to a very different regime occurs. For $\kappa > 6$ the spectra of the angular

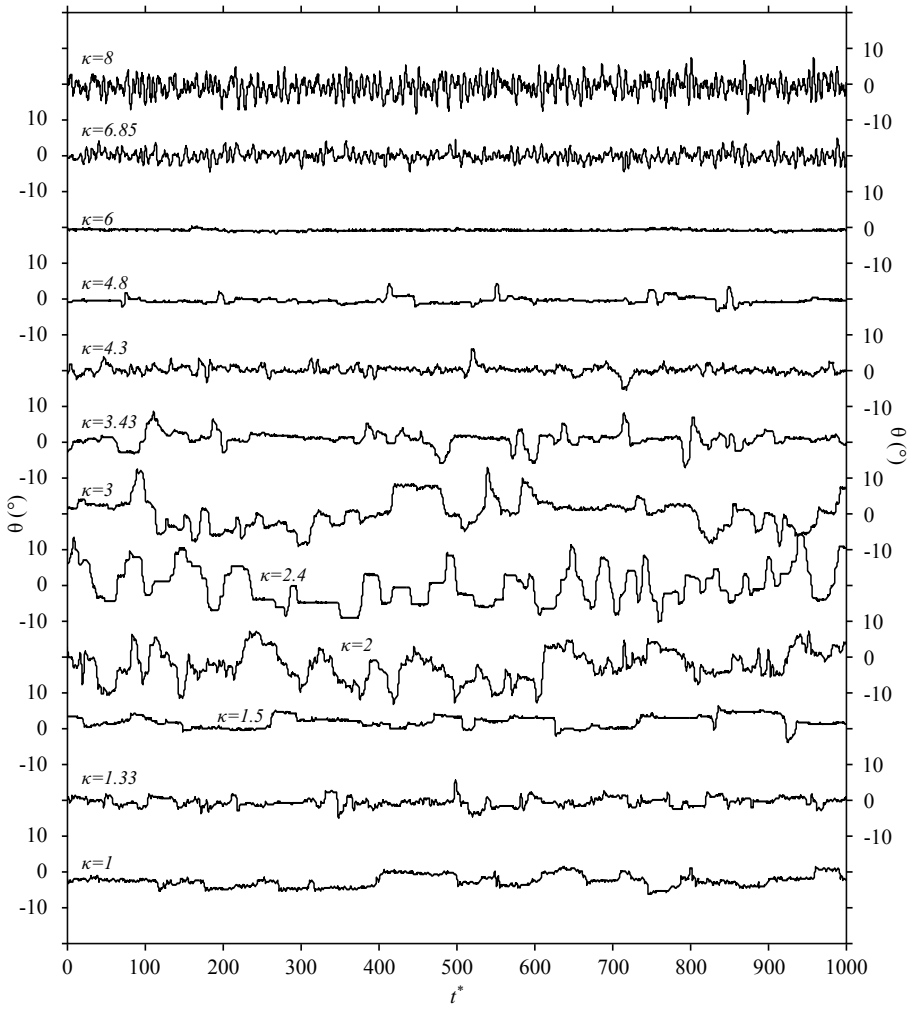

FIGURE 7. Time series of the angular position $\theta(t^*)$ for $\kappa = [1 - 8]$ in descending order from top to bottom.

position look like the response of a linear oscillator to a random excitation having an eigen frequency of St= 0.14.

The high frequency peaks in the spectrum obtained for $\kappa = 8$ are suspected to originate from the vortex shedding of the plate that is comparable to a square cylinder with $W = 6$ mm sides. The highest frequency peak at St= 1.4 provides a Strouhal number based on W, $St_W = 0.175$ that is reasonable for this assumption. The motion can be caused by a rotation around the long axis of symmetry of the plate due to the small gap clearance around the cylindrical support as well as a sliding motion in the z direction.

4. Discussion and concluding remarks

For aspect ratio $\kappa < 6$, the long time dynamics of the angular position (for frequencies $f^* < 0.2$) is fully stochastic (i.e. no periodicity) with random appearances of high angular velocities. It is shown that static symmetry breaking modes of the wake are responsible for the plate dynamics. Using a global stability analysis of the flow past rectangular

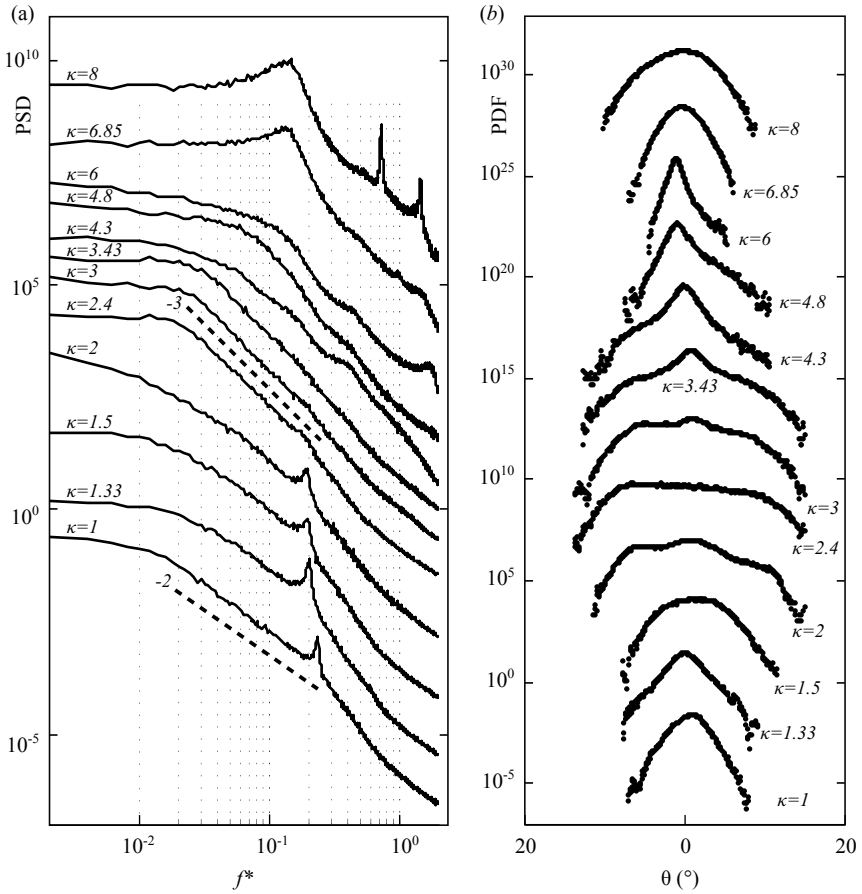

FIGURE 8. Power spectra (a) and probability density function (b) of the angular position $\theta(t^*)$ for $\kappa = [1 - 8]$ in descending order from top to bottom. In (a) frequencies in non dimensional units are defined as $f^* = fH/U_0$, dashed lines are -2 and -3 power laws.

plates, Marquet & Larsson (2014) predicted the presence of steady symmetry breaking modes as soon as $\kappa < 2.5$ and Reynolds number Re> 150. There is then an agreement about the presence of the modes at low aspect ratios leading to a transition when the aspect ratio is increased. The larger critical aspect ratio obtained in the experiment can be ascribed to many effects such as the large Reynolds number, the plate motion, the large blockage in the hydrodynamic tunnel and the cylinder axis presence.

The PDFs in Fig. 8(b) are almost uniform meaning that the dynamics is here multistable (see the succession of steady angles in the dynamics displayed in Fig.7). From the low Reynolds number study of Marquet & Larsson (2014), we actually would expect four modes, a pair of static modes for each axis symmetry breaking. For a sake of simplicity, they can be roughly reduced to one asymmetric spatial mode but with a variable azimuthal phase that can take four values. The static modes in a pair are then just π shifted from each other (mirror modes, denoted P and N). On a more practical point of view, the azimuthal phase of the mode indicates the torque orientation exerted on the body. For our experiment, only both the mode P and N of the small symmetry axis breaking lead to a change of the angular positions of the plate, while the two modes of the long symmetry axis breaking do not have any effect on θ. If the four corresponding azimuthal phases are equally explored during the turbulent dynamics, one would then

expect a symmetric three-modal angle distribution with a probability for $\theta = 0$ to be twice the probability at either $\theta > 0$ or $\theta < 0$. It is clearly not the case, however the distributions obtained for $\kappa = 2, 3$ in Fig. 8(b) with their three weak bumps may present some similitude with this expectation. Since the distributions are almost uniform, it is likely that the wake dynamics is more similar to that of an axisymmetric body as recently evidenced by Rigas *et al.* (2015). In that case, the dynamics is a combination of random noise of the azimuthal phase of the static mode together with π phase jumps toward the mirror static mode. The appearances of the modulation in the angular distribution is perhaps due to a small preferences toward azimuthal phase selections compatible with the two reflectional symmetries of the plate.

It is speculated that the projection of the resulting fluid force of the wake dynamics on the only degree of freedom θ of our simple mechanical system can produce the observed dynamics. The low order model based on Langevin equation presented by Rigas *et al.* (2015) will be the next step to investigate the modelling of this stochastic fluid structure interaction.

Finally, it is noteworthy that for the low aspect ratios ($\kappa < 6$), the classical periodic vortex shedding (observed here at Strouhal numbers $\mathrm{St} \simeq 0.235 - 0.195$) reminiscent from the Hopf bifurcation at low Reynolds number is relegated as a second order contribution to the dynamics emphasizing the dominant strength of the asymmetric static modes and their related stochastic dynamics for large Reynolds numbers.

Acknowledgments

The work has been motivated by a fruitfull discussion with F. Gallaire and O. Marquet during the 6th International Symposium on Bifurcation and Instabilities in Fluid Dynamics. The author wish to thank O. Doaré for the critical reading of the manuscript and for drawing his attention on a characterization of the solid friction.

REFERENCES

Bohorquez, P., Sanmiguel-Rojas, E., Sevilla, A., Jiménez-González, JI & Martínez-Bazán, C. 2011 Stability and dynamics of the laminar wake past a slender blunt-based axisymmetric body. *Journal of Fluid Mechanics* **676** (1), 110–144.

Ern, Patricia, Risso, Frederic, Fabre, David & Magnaudet, Jacques 2012 Wake-Induced Oscillatory Paths of Bodies Freely Rising or Falling in Fluids. *Annual Review of Fluid Mechanics* **44**, 97–121.

Fabre, D., Auguste, F. & Magnaudet, J. 2008 Bifurcations and symmetry breaking in the wake of axisymmetric bodies. *Physics of Fluids* **20**, 051702.

Grandemange, M., Gohlke, M. & Cadot, O. 2012 Reflectional symmetry breaking of the separated flow over three-dimensional bluff bodies. *Physical Review E* **86**, 035302.

Grandemange, M., Gohlke, M. & Cadot, O. 2013 Turbulent wake past a three-dimensional blunt body. Part 1. Global modes and bi-stability. *Journal of Fluid Mechanics* **722**, 51–84.

Grandemange, M., Gohlke, M. & Cadot, O. 2014 Statistical axisymmetry of the turbulent sphere wake. *Experiments in fluids* **55** (11), 1–10.

Marquet, O. & Larsson, M. 2014 Global wake instabilities of low aspect-ratio flat-plates. *European Journal of Mechanics B/Fluids* **49** (-1), 400–412.

Pier, B. 2008 Local and global instabilities in the wake of a sphere. *Journal of Fluid Mechanics* **603**, 39–61.

Rigas, G., Morgans, A.S., Brackston, R. D. & Morrison, J.F. 2015 Diffusive dynamics and stochastic models of turbulent axisymmetric wakes. *Journal of Fluid Mechanics* **778**, R2.

Rigas, G., Oxlade, A.R., Morgans, A.S. & Morrison, J.F. 2014 Low-dimensional dynamics of a turbulent axisymmetric wake. *Journal of Fluid Mechanics* **755**, 159.

Wu, T 1956 A free streamline theory for two-dimensional fully cavitated hydrofoils. *Journal of Mathematics and Physics* **35** (1), 236–265.